

<sup>6</sup>B. Lax and J. G. Mavroides, in *Solid State Physics*, edited by H. Ehrenreich, F. Seitz, and D. Turnbull (Academic, New York, 1960), Vol. 11, p. 368.

<sup>7</sup>E. J. Tichovol'sky and J. G. Mavroides, *Solid State Commun.* **7**, 927 (1969).

<sup>8</sup>L. C. Hebel and P. A. Wolff, *Phys. Rev. Lett.* **11**, 368 (1963).

<sup>9</sup>G. E. Smith, G. A. Baraff, and J. M. Rowell, *Phys.*

*Rev.* **135**, A1118 (1964).

<sup>10</sup>B. E. Meierovich, *Zh. Eksp. Teor. Fiz.* **58**, 1412 (1970) [*Sov. Phys. JETP* **31**, 756 (1970)].

<sup>11</sup>H. D. Drew and U. Strom, *Phys. Rev. Lett.* **25**, 1755 (1970).

<sup>12</sup>V. S. Edel'mann and S. M. Cheremisin, *Pis'ma Zh. Eksp. Teor. Fiz.* **11**, 373 (1970) [*JETP Lett.* **11**, 250 (1970)].

## Polarized Raman Scattering in Transparent Polycrystalline Solids\*

W. J. Brya

*Sandia Laboratories, Albuquerque, New Mexico 87115*

(Received 19 February 1971)

The polarized Raman spectra of transparent polycrystalline solids are shown to provide results essentially identical to those obtainable from single-crystal Raman studies. Analytic expressions for the polarized scattering functions are obtained and, by way of illustration, are used to determine the symmetries and frequencies of many of the phonon modes for several transparent (Pb, La)(Zr, Ti)O<sub>3</sub> ceramics in the tetragonal ferroelectric phase.

In a recent Letter<sup>1</sup> it was shown that the unpolarized Raman scattering from ceramic systems contains the basic features of Raman scattering in the single-crystal material. With the aid of PbTiO<sub>3</sub> Raman data,<sup>2</sup> a detailed study of the lattice dynamics of the Pb(Zr, Ti)O<sub>3</sub> or PZT ceramic was carried out. In the present paper we show that the *polarized* Raman scattering in transparent piezoelectric ceramics permits the determination of many phonon frequencies and symmetries without the need for single-crystal data. The application of the theoretical results to the transparent (Pb, La)(Zr, Ti)O<sub>3</sub> or PLZT ceramics<sup>3</sup> demonstrates the additional advantages of this technique over the previous one for selected systems.

*Ceramic spectral functions.*—Although the effect to be described is quite general, the detailed calculations are usually dependent on the crystal structure. Consequently, we confine ourselves to a discussion of the Raman spectra of the PZT/PLZT ceramics in the tetragonal  $C_{4v}$  phase. The twelve optic modes in the high-temperature cubic phase consist of three triply degenerate  $F_{1u}$  modes (infrared active and Raman inactive) and a single triply degenerate  $F_{2u}$  mode (Raman and infrared inactive) which become  $3A_1+3E$  and  $B_1+E$  modes, respectively, in the  $C_{4v}$  state. These latter modes are all Raman active and all, except  $B_1$ , are infrared active. The long-range electrostatic forces associated with the infrared activity further split the modes

into longitudinal and transverse components and several modes show frequencies dependent on their directions of propagation in the crystallites. For a general direction, the  $A_1+E$  modes comprise one transverse  $E(TO)$  mode of constant frequency and two mixed modes of combined  $A_1+E$  symmetry with variable frequency; for propagation parallel or perpendicular to the crystallite  $c$  axis, the mixed modes attain their limiting frequencies and become pure  $E(LO)$  and  $A_1(LO)$  or  $A_1(TO)$  and  $E(LO)$  modes, respectively. For the  $B_1+E$  modes one obtains a transverse  $E(LO)$  mode and a mixed  $B_1$  mode, each of constant frequency, and a mixed  $E$  mode of variable frequency which becomes an  $E(LO)$  or  $E(LO)$  mode for propagation along or normal to the  $c$  axis, respectively.

We consider right-angle scattering in a ceramic relative to a laboratory-fixed orthogonal reference system  $xyz$ ; the incident laser beam and scattered light are directed along  $x$  and  $y$ , respectively. We assume a transparent medium with small birefringence, such that the propagation directions and polarizations of incident and scattered light are conserved. Using the expressions of Loudon,<sup>4</sup> one readily determines the scattering efficiency  $S(\theta, \varphi, \psi)$  of a particular mode for a given crystallite in the ceramic; here the Eulerian angles  $\theta$ ,  $\varphi$ , and  $\psi$  fix the orientation of the crystallite relative to the laboratory system. In a ceramic comprised of randomly oriented crystallites, the scattering

from crystallites of a given orientation is proportional to the probability,  $\rho(\theta, \varphi, \psi) = \rho(0) - (8\pi^2)^{-1} \times \sin\theta$ , of occurrence of the orientation (where  $\theta$  is the angle between the crystallite  $c$  axis and the laboratory  $z$  axis); the total scattering efficiency  $S$  of a mode is then obtained by a suitable integration over the angles, i.e.,  $S = \iiint S(\theta, \varphi, \psi) \times \rho(\theta) d\theta d\varphi d\psi$ . For the incident and scattered beams polarized along principal axes of the  $xyz$  system, there are only two independent scattering geometries; the scattering efficiency  $S_{\perp}$  for incident and scattered beams polarized normal to the scattering plane [ $x(zz)y$  scattering in the usual single-crystal notation<sup>5</sup>] and the scattering efficiency  $S_{\parallel}$  for incident and scattered beams polarized normal to each other [ $x(zx)y$ ,  $x(yz)y$ , or  $x(yx)y$  scattering].

Using the above expressions, it is relatively easy to show that scattering from the fixed-frequency  $E(\text{TO})$  and  $B_1$  modes is essentially depolarized with  $S_{\parallel}/S_{\perp} = 0.75$ ; polarization studies, therefore, yield little information about these modes and, as shown later, the scattering may add further confusion to the spectral interpretation. Scattering from the mixed modes is of more interest since the intensity is now spread over a frequency interval bounded by the limiting values occurring for phonon propagation parallel and normal to the crystal  $c$  axis. In this case, the scattering intensity  $S$  is uninformative, and a determination of the scattering intensity per unit frequency interval,  $S(\omega)$ , is needed.

The mixed phonon frequencies and polarizations for a given direction are determined by the relative importance of the anisotropic short-range interatomic forces and the long-range electrostatic forces.<sup>4</sup> The general expressions for the phonon properties are difficult to handle analytically so we consider just those cases where either the short- or long-range forces dominate. For the mixed  $A_1 + E$  modes, wherein the long-range forces prevail, the phonons are essentially longitudinal and transverse with frequencies<sup>4</sup>

$$\begin{aligned} \omega_{\text{LO}}^2 &= \omega_{A_1(\text{LO})}^2 \cos^2\chi + \omega_{E(\text{LO})}^2 \sin^2\chi, \\ \omega_{\text{TO}}^2 &= \omega_{E(\text{TO})}^2 \cos^2\chi + \omega_{A_1(\text{TO})}^2 \sin^2\chi, \end{aligned} \quad (1)$$

where  $\chi$  is the angle between the direction of propagation and the  $c$  axis. By expressing  $\chi$  in terms of the Eulerian angles, one can introduce a variable transformation and thereby obtain the required density function  $S(\omega)$ . The calcula-

tions are slightly tedious and the results are too lengthy to be presented here. Instead we present in Figs. 1(a) and 1(b) characteristic forms for  $S_{\perp}(\omega)$  and  $S_{\parallel}(\omega)$  over normalized frequency intervals. The shapes of the functions, except at the extrema, are dependent on a number of parameters: the relative values of the Raman-polarizability-tensor components  $\alpha_{ij}$  and the relative strengths  $\alpha^2$  and  $\beta^2$  of the scattering intensities arising from the deformation-potential electron-phonon interaction and from the polar electron-phonon mechanism associated with the electro-optic properties of the material. For our examples  $\alpha_{xx}(A_1) = \alpha_{yy}(A_1) = 2.0$ ,  $\alpha_{zz}(A_1) = 1.0$ , the nonzero  $\alpha_{ij}(E)$  satisfy  $\alpha_{ij}(E) = 1.0$ , and  $\alpha^2 = \beta^2 = 1.0$ . One notes the pronounced differences in the spectra of  $S_{\perp}$  and  $S_{\parallel}$ , particularly at the extremes. For  $\omega_{E(\text{LO})}$  [ $S_{\parallel}$ ] and  $\omega_{A_1(\text{TO})}$  [ $S_{\parallel}$  and  $S_{\perp}$ ], the singularities vary as  $|\omega^2 - \omega_c^2|^{-1/2}$  near the limiting frequency  $\omega_c$ ; near  $\omega_{E(\text{LO})}$  [ $S_{\perp}$ ] the intensity goes to zero as  $|\omega^2 - \omega_c^2|^{1/2}$ . Both func-

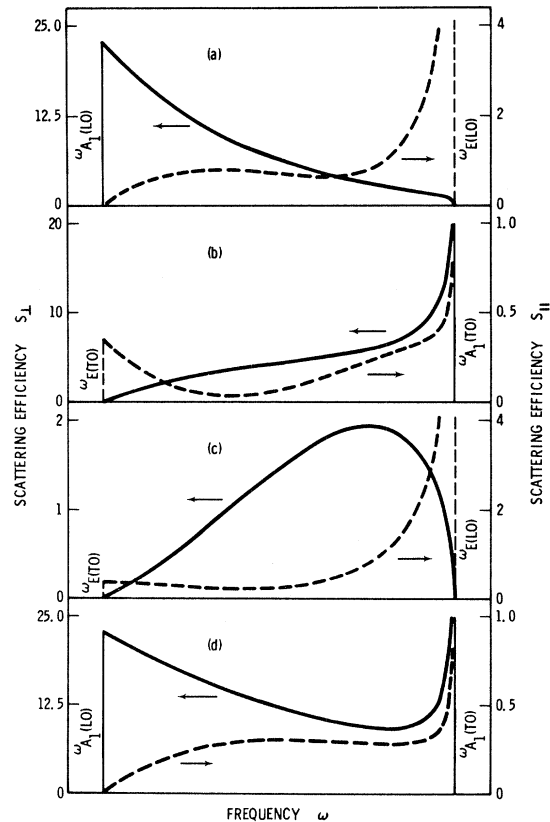


FIG. 1. Characteristic polarized Raman spectra of ceramics for variable-frequency phonon modes of the  $C_{4v}$  crystal class. The scattering geometries  $S_{\perp}$  (solid curves) and  $S_{\parallel}$  (dashed curves) are discussed in the text. (a), (b) Long-range electrostatic forces dominate the short-range interatomic forces; (c), (d) short-range forces dominate.

tions produce rapid changes in the scattering intensity at the extrema. The spectra at  $\omega_{A_1(LO)}$  [ $S_{\perp}$ ] and  $\omega_{E(TO)}$  [ $S_{\parallel}$ ] have finite values for  $S(\omega)$  and also show noticeable intensity changes at  $\omega_c$ ; for  $\omega_{A_1(LO)}$  [ $S_{\parallel}$ ] and  $\omega_{E(TO)}$  [ $S_{\perp}$ ], however, the  $S(\omega)$  go to zero as  $|\omega^2 - \omega_c^2|$  and no pronounced changes are expected.

When the short-range forces dominate, the mixed  $A_1 + E$  modes are characterized by phonons of symmetries  $A_1$  and  $E$  with polarizations essentially parallel and perpendicular to the  $c$  axis and the phonon frequencies become<sup>4</sup>

$$\omega_E^2 = \omega_{E(TO)}^2 \cos^2 \chi + \omega_{E(LO)}^2 \sin^2 \chi, \quad (2a)$$

$$\omega_{A_1}^2 = \omega_{A_1(LO)}^2 \cos^2 \chi + \omega_{A_1(TO)}^2 \sin^2 \chi. \quad (2b)$$

One performs a variable transformation to determine  $S(\omega)$  and obtains the results of Figs. 1(c) and 1(d). At the extrema the spectra show the same functional dependences on frequency as obtained for Eq. (1).

The mixed  $E$  mode associated with the  $B_1$  mode is a pure symmetry mode irrespective of the relative strengths of the long- and short-range forces. Its frequency therefore varies as Eq. (2a) and the spectra have the forms of Fig. 1(c). For the  $E$  modes derived from the  $F_{2u}$  mode of the cubic phase, the infrared activity in the  $C_{4v}$  state may be small.<sup>6</sup> Thus the expected  $B_1$ - $E(TO)$ - $E(LO)$  mode splittings may also be small and lead to apparent mode degeneracies in the spectra; then the scattering from the degenerate modes will become depolarized with  $S_{\parallel}/S_{\perp} \approx 0.75$ . In addition, the spectra may be further complicated by the depolarized scatterings from the fixed-frequency  $E(TO)$  modes discussed earlier, and additive depolarized scattering singularities are introduced into Figs. 1(b) and 1(c) at the frequencies  $\omega_{E(TO)}$ . Also line broadening effects arising from phonon damping, etc. may cause a smoothing out of the sharp structure.

*Polarized scattering in PLZT ceramics.*—The PLZT ceramic samples<sup>7</sup> were prepared using the techniques detailed by Haertling and Land.<sup>3</sup> For the samples of interest, an increasing concentration of Zr and/or La leads to a lowering of the Curie temperature; introduction of significant Zr produces a ferroelectric rhombohedral phase while appreciable substitution of La leads to a nonferroelectric cubic phase. The right-angle Raman spectra were obtained using an argon-ion laser, a double-grating spectrometer, and a cooled phototube operating in the photon-counting mode. All measurements were made at

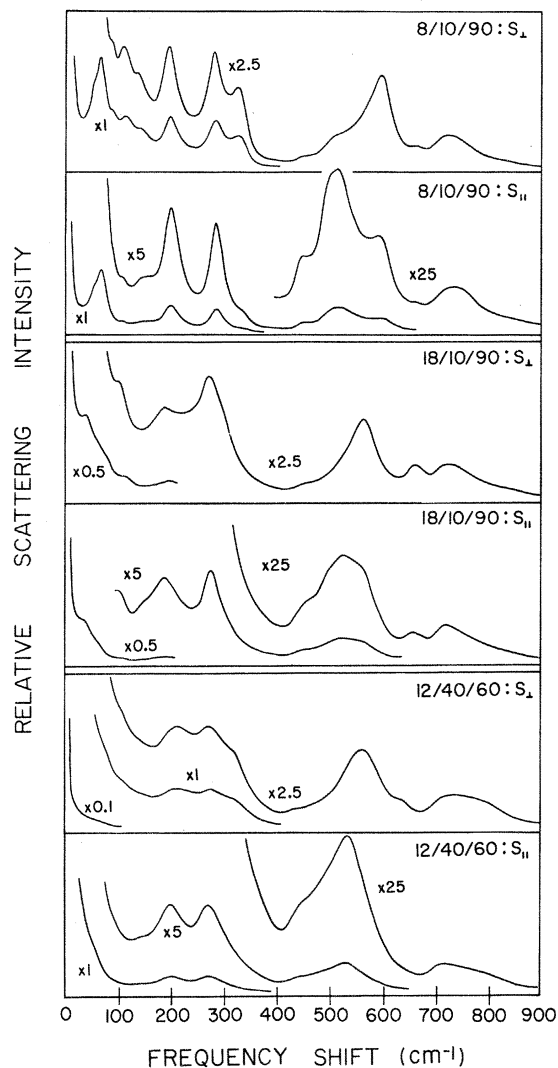


FIG. 2. Experimental polarized Raman spectra for tetragonal  $(Pb, La)(Zr, Ti)O_3$  ceramics at room temperature. Scattering geometries and sample notation are explained in text. Note the gain changes throughout the spectra. Mode symmetries and frequencies are listed in Table I.

room temperature with an instrumental resolution of  $6 \text{ cm}^{-1}$ .

Figure 2 shows spectra of  $S_{\perp}$  and  $S_{\parallel}$  obtained for materials of compositions 8/10/90, 18/10/90, and 12/40/60. (The sample notation specifies the percentage concentrations of La/Zr/Ti, respectively, in the ceramic.) The  $S_{\parallel}$  spectra are obtained using the  $x(vx)y$  scattering geometry; this configuration minimizes the leakage of the stronger  $S_{\perp}$  spectrum into the weaker  $S_{\parallel}$  which occurs when the intrinsic birefringence of the material depolarizes the incident and scattered beams. The differences in the shapes and intensities of

Table I. Optical-phonon assignments for several tetragonal (Pb, La)(Zr, Ti)O<sub>3</sub> ceramics at room temperature. Sample notation denotes percentage concentration of La/Zr/Ti in ceramic.

Phonon mode symmetry	Phonon frequencies (cm <sup>-1</sup> )		
	Sample compositions		
	8/10/90	18/10/90	12/40/60
1E(TO)	65	...	
1A <sub>1</sub> (TO)	85	...	
1E(LO)	135	~135	~135
1A <sub>1</sub> (LO)	~195	~190	210
2E(TO)	195	190	195
2A <sub>1</sub> (TO)	330	~300	320
2E(LO)	445	440	~430
2A <sub>1</sub> (LO)	~495	~495	~500
B <sub>1</sub> } 3E(TO) 3E(LO)	280	275	270
4E(TO)			
4A <sub>1</sub> (TO)	595	565	560
4E(LO)	~710	715	710
4A <sub>1</sub> (LO)	~750	~740	795

the spectra for the two geometries are clearly evident, particularly in the regions of 325 and 550 cm<sup>-1</sup>, and the scattering is readily analyzed on the basis of our theoretical results. In Table I we list the various phonon symmetries and frequencies for these materials; the symmetry assignments are based on the model for which the long-range forces dominate. The results are in good agreement with previously published data on the Raman<sup>2</sup> and infrared<sup>8</sup> spectra of single-crystal PbTiO<sub>3</sub>, and unpolarized Raman spectra in PZT ceramics.<sup>1,8</sup> Our polarized spectra are especially useful in resolving closely spaced phonon modes. (The triply degenerate mode at ~275 cm<sup>-1</sup> derives from the  $F_{2u}$  mode of the high-temperature cubic phase as previously discussed.) The "soft" 1E(TO) and 1A<sub>1</sub>(TO) modes<sup>1,2</sup> were observed only in the 8/10/90 material; their absence in the samples of lower Curie temperatures is probably due to the much lower frequencies and/or possible overdamping of the modes. The features observed at 40, 75, and 110 cm<sup>-1</sup> are apparently second-order lines and are in good agreement with the neutron-scattering results of Shirane *et al.*<sup>9</sup> for PbTiO<sub>3</sub>. The line at ~650 cm<sup>-1</sup>, which is quite pronounced in the 18/10/90 material, is believed to be an "impurity" mode associated with the introduction of La (with its necessary charge compensation) into the lattice. With the exception of the soft

E(TO) mode, the E modes generally show little frequency shift with a variation of material composition, while the A<sub>1</sub> modes are typically more sensitive to such changes; this behavior is also consistent with previous work.<sup>1</sup> In addition, the shapes and intensities of the spectra allow reasonable estimates of the polarizability-tensor components, and one typically finds that  $\alpha_{xx}(A_1) = \alpha_{yy}(A_1) \approx \alpha_{zz}(A_1)$  and that (nonzero)  $\alpha_{ij}(E) < \alpha_{xx}(A_1), \alpha_{zz}(A_1)$ . The scattering intensities of the LO phonons are consistently less than those of the TO modes, indicating that the usual deformation-potential scattering experiences some cancellation by the polar-scattering mechanism.

Further studies throughout the compositional phase diagram (at various temperatures) will provide considerable information on the lattice dynamics of the PLZT solid-solution system and the more familiar PZT system. In particular, detailed studies in the ferroelectric rhombohedral phases and the antiferroelectric phase should lead to a better understanding of the PbZrO<sub>3</sub> system. Burns and Scott<sup>1</sup> report the occurrence of broad, rather featureless spectra for the PZT ceramics in the rhombohedral phases; they tentatively attribute these to second-order scattering. Our preliminary measurements in 9/65/35 PLZT, which is also rhombohedral, show the same broad spectra; however, the S<sub>⊥</sub> and S<sub>∥</sub> spectra are decidedly different and assignments of phonon symmetries and frequencies should be possible.

In conclusion, we find that the polarized Raman spectra of transparent piezoelectric ceramics yield results essentially identical to those obtainable from single-crystal studies. The ceramic data allow a direct determination of many of the mode symmetries and frequencies and reasonable estimates of the relative importance of long- and short-range forces, of the relative strengths of the polarizability tensor components, and of the effect of the polar-scattering mechanism on LO-mode scattering intensities—all without recourse to single-crystal data. Although there is no substitute for the information to be obtained from single-crystal studies, the usefulness of this ceramic technique to those systems for which single crystals are not available is clear.

We gratefully acknowledge the aid of G. H. Haertling, C. E. Land, and I. D. McKinney in sample fabrication and preparation, and a number of useful discussions with J. P. VanDyke on the theory.

\*Work supported by the U. S. Atomic Energy Commission.

<sup>1</sup>G. Burns and B. A. Scott, Phys. Rev. Lett. **25**, 1191 (1970).

<sup>2</sup>G. Burns and B. A. Scott, Phys. Rev. Lett. **25**, 167 (1970).

<sup>3</sup>G. H. Haertling and C. E. Land, J. Amer. Ceram. Soc. **54**, 1 (1971).

<sup>4</sup>R. Loudon, Advan. Phys. **13**, 423 (1964).

<sup>5</sup>T. C. Damen, S. P. S. Porto, and B. Tell, Phys. Rev. **142**, 570 (1966).

<sup>6</sup>M. DiDomenico, Jr., S. H. Wemple, S. P. S. Porto, and R. P. Bauman, Phys. Rev. **174**, 522 (1968).

<sup>7</sup>The favored compositional formula for the PLZT system is  $Pb_{1-x}La_x(Zr_yTi_{1-y})_{1-x/4}O_3$ , which assumes that the charge compensation necessitated by the substitution of La for Pb is brought about by vacancies in the (Zr, Ti) sites (see Ref. 3).

<sup>8</sup>N. E. Tornberg and C. H. Perry, J. Chem. Phys. **53**, 2946 (1970).

<sup>9</sup>G. Shirane, J. D. Axe, J. Harada, and J. P. Remeika, Phys. Rev. B **2**, 155 (1970).

## Reaction Mechanism for $p$ -Wave Neutron Capture in $Mo^{92}$ and $Mo^{98}$ †

S. F. Mughabghab, R. E. Chrien, O. A. Wasson, G. W. Cole, and M. R. Bhat

Brookhaven National Laboratory, Upton, New York 11973

(Received 3 March 1971)

A study of  $\gamma$ -ray intensities following neutron capture in  $Mo^{92}$  and  $Mo^{98}$  provides evidence for a simple reaction mechanism which dominates the decay of the compound nuclear state. The intensities are largely accounted for by the motion of a valency neutron in transitions of the type  $p_{3/2} \rightarrow d_{3/2}$ ,  $d_{5/2}$ , or  $s_{1/2}$ , and  $p_{1/2} \rightarrow s_{1/2}$  or  $d_{3/2}$ .

In recent years, evidence has been accumulating that simple reaction mechanisms play a significant role in slow-neutron radiative capture.<sup>1-7</sup> These mechanisms manifest their presence through correlations between reaction widths. One such simple mechanism is the channel-capture effect, or valency-neutron model, suggested by Lane and Lynn<sup>8</sup> and Lynn.<sup>9</sup> This model assumes that the radiative widths for neutron resonances may be calculated by considering the motion of a single neutron in a potential well; the contribution of core transitions is neglected. Such a description has validity only if the final state for the moving neutron has a preponderantly single-particle character, and in this case one can write, for electric dipole  $\gamma$ -ray emission, using the notation of Ref. 9,

$$\Gamma_{\lambda\mu} = \frac{16\pi k^3}{9} \theta_\lambda^2 \theta_\mu^2 \left| \bar{e} \int_0^\infty dr u_\lambda r u_\mu \right|^2 \frac{|\langle j' I J_\lambda || Y^{(1)} || j'' I J_\mu \rangle|^2}{2J_\lambda + 1}, \quad (1)$$

where the reduced matrix element for the operator  $Y^{(1)}$  can be written

$$\frac{|\langle j' I J_\lambda || Y^{(1)} || j'' I J_\mu \rangle|^2}{2J_\lambda + 1} = \frac{3}{4\pi} (2J_\mu + 1)(2j' + 1)(2j'' + 1)(2l' + 1) W^2(j' J_\lambda j'' J_\mu; I1) \\ \times W^2(l' j' l'' j''; \frac{1}{2} 1) C^2 \mu_1(l'' 0; 00). \quad (2)$$

This model predicts a correlation between the radiative width and the dimensionless reduced widths of the initial and final states,  $\theta_\lambda^2$  and  $\theta_\mu^2$ . Although evidence has been obtained in several nuclides for a correlation between radiative widths and neutron widths for the initial states (i.e., the neutron resonances), a detailed experimental verification of Eq. (1) has never been achieved. This fact is undoubtedly due to the small widths predicted by (1) for medium- and heavy-mass targets. The effect of valency-neutron transitions is masked by more complex processes occurring in compound-nucleus decay.

In this Letter we report quantitative verifica-

tion of the valency-neutron-transition model for neutron capture in  $p$ -wave resonances of  $Mo^{92}$  and  $Mo^{98}$ , leading to final  $s$  and  $d$  states in  $Mo^{93}$  and  $Mo^{99}$ , respectively. These cases are favorable to the valency-neutron model since  $Mo^{92}$  has shell closure at  $N = 50$ , while in  $Mo^{98}$  the  $d_{5/2}$  shell is similarly filled.

Measurements have been carried out at the Brookhaven high-flux-beam reactor fast-chopper facility on enriched samples of  $Mo^{92}$  and  $Mo^{98}$ . A  $\gamma$ -ray resolution of 5 keV out of 6 MeV was achieved. Earlier measurements of our own group,<sup>10-12</sup> and those of others,<sup>13</sup> had already in-